Study on $LiNbO_3$ channel and ridge waveguides - based on helium ion implantation combined with lithography and precise diamond dicing

Sumei Wang (王素梅)[1], Jinhua Zhao (赵金花) [1,*], Jinjun Gu (谷金军)[1], Mingyang Bu (卜铭洋)[1], Li Fan (范丽)[1], Shuang Li (李爽)[1], Xifeng Qin (秦希峰)[1], Yicun Yao (姚一村)[2], Yingying Ren (任莹莹)[3], Lei Wang (王磊)[4]

[1]School of Science, Shandong Jianzhu University, Jinan 250101, China
[2]Shandong Key Laboratory of Optical Communication Science and Technology, School of Physical Science and Information Technology, Liaocheng University, Liaocheng 252059, China
[3]Shandong Provincial Engineering and Technical Center of Light Manipulations & Shandong Provincial Key Laboratory of Optics and Photonic Device, School of Physics and Electronics, Shandong Normal University, Jinan 250014, China
[4]School of Physics, Shandong University, Jinan 250100, China
**Corresponding author: zhaojinhua@sdjzu.edu.cn*

Received Month X, XXXX; accepted Month X, XXXX; posted online Month X, XXXX

Lithium niobate channel and ridge waveguides have been successfully fabricated by the He ion implantation, which have an energy of 500 keV and a fluence of 1.5×10^{16} ions/cm^2 that combined with lithography and precise diamond dicing technique. The refractive index profile of the annealed LN planar waveguide was reconstructed. The propagation loss of the channel waveguide with a width of 10 μm and that of the ridge waveguides with widths of 25 μm and 15 μm were investigated by the end-face coupling method. In our work, the factors that affect the waveguide properties of channel and ridged waveguides were revealed.
OCIS Codes: 130.3730, 160.4760, 230.7390.

1. Introduction

In recent decades, lithium niobate ($LiNbO_3$, LN), with an oxygen octahedral structure, has been applied in photonic industry and considered to be optical "silicon"[1, 2] for its unique properties – namely excellent electro-optic, nonlinear optical properties, wide transparency window, exceptional signal quality and good temperature stability [3-4]. Lithium niobate on insulator (LNOI) platform promises to combine the excellent nonlinear properties of LN crystal with high contrast waveguides [5]. Recent progress in fabrication technique has enabled ultra-low loss thin film LN waveguides, which is revolutionizing not only the LN industry, but also the field of large-scale photonic integration [6]. As a result, the LN crystals are found in a wide range of experiments and optical devices[2], so they were researched in this paper.

As an essential unit of integrated optical circuits, optical waveguides can limit and transmit light waves in the order of square microns by using the principle of total reflection at the interface of two materials with different refractive indices [7]. Planar waveguide is the simplest and easiest to prepare, but it only limits the optical field in one direction. Two-dimensional (2D) waveguides such as channel waveguide and ridge waveguide have been investigated to restrict the waveguide in both horizontal and vertical directions, reduce the propagation loss, and be easier to connect with other optical elements in most cases. In the past few decades, much effort has gone into developing LN 2D waveguide structures and many papers have been published on this topic [8-13]. Among them, optical waveguides have been successfully used in various optical devices, such as optical switches [8,9], power splitters [10-12], and polarization beam splitters [13].

The main methods used to prepare optical waveguide structures in $LiNbO_3$ crystals are metal in-diffusion, proton exchange, ion implantation, femtosecond laser writing, and so on [14,15]. Ion implantation technology is based on the interaction between ions and solids and has strong controllability and repeatability. Since it was used in material surface modification and material analysis in the 1960s, it has been paid much attention by researchers and successfully applied to various materials [16]. In recent years, helium (He) ion implantation has attracted much attention and interest in diverse materials [17-19]. Compared with the heavy ion implantation, the waveguide formed by He ion implantation has less damage in the guidance zone and higher penetration depth. The low energy (such as several hundred keV) He ion implantation was chosen to fabricate a single-mode waveguide, which has many applications in practical devices [20]. However, ion implantation can only form planar waveguides. Fabrications of channel waveguides and ridge waveguides require combinations of other methods. In this work, the channel waveguide was fabricated by He ion implantation combined with lithography, whilst the ridge waveguide was prepared by precise diamond dicing based on an annealed planar waveguide. Precise diamond dicing can be used to create highly confined optical waveguides. And the width of the ridge waveguide fabricated on the bulk LN by the method can be as small as 1 μm [21]. LN planar waveguides, channel waveguides, and ridge waveguides have been studied extensively [22-24], but, to our knowledge,

no paper has compared channel waveguides and ridge waveguides under the same conditions so far. In this work, the major attention is devoted to analysing the refractive index of LN waveguides and to comparing the channel waveguide and the ridge waveguides from waveguide quality.

2. Experiment

To fabricate waveguides in LN crystals, z-cut optical grade LN crystals with the size of 12 mm × 9 mm × 1 mm were cleaned and implanted; the implantation energy was 500 keV, and the implantation fluence was 1.5×10^{16} ions/cm^2 at room temperature. During ion implantation, the samples were titled by 7° off the incident beam direction to prevent the channeling effect. The samples were annealed at 260°C in the air for 30 minutes after ion implantation to improve guiding quality.

The schematics of the fabrication process for channel and ridge waveguides are illustrated in Figs. 1(a) and 1(b), respectively. As shown in Fig. 1(a), the channel waveguide was obtained by using standard lithography technology and the He ion implantation process. The thickness of the photoresist mask (BP-218) is sufficient to block high-energy ions, the openings (~10 μm) where ions can pass freely and be implanted into the LN substrate. After standard lithography process, we obtained a photoresist mask of open strips 10 μm in width with a period of 50 μm. He ions were implanted into the unshielded region to obtain the channel waveguide (WG10). For comparison, the implantation (500 keV He ions, 1.5×1016 ions/cm2) and subsequent annealing conditions (260°C for 30 minutes) of all samples were consistent.

The preparation of the ridge waveguide consisted of two steps, first obtaining the planar waveguide layer, and then forming the ridges in specific areas by precise diamond dicing. The second step of the process is shown in Fig. 1(b). The cutting speed of the precision diamond blade is 40,000 rpm and the moving speed is 0.5 mm /s. The width of the diamond blade used in the experiment was 50 μm. Two microgrooves were fabricated by using the diamond tool in one direction relative to the LN crystal, and a ridge waveguide was formed between the two microgrooves. Two kinds of the ridges were prepared with widths of 15 μm (WG15) and 25 μm (WG25) in the same LN crystal for direct comparison, but only the ridges with a width of 15 μm are shown in Fig. 1(b).

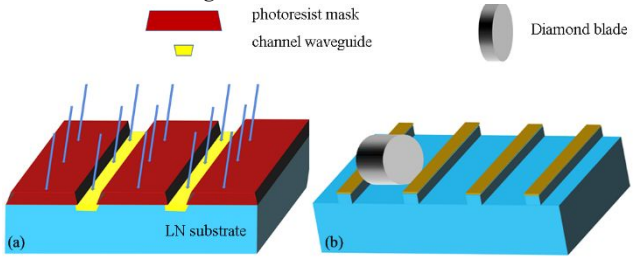

Fig. 1. Fabrication methods of LN waveguides: (a) channel guide; (b) ridge guide.

The displacement per atom (dpa) was calculated by using the calculation software for the stop and range of ions in matter (SRIM) 2013, and the refractive index profiles (RIPs) of the waveguides were reconstructed. Then, the dark-mode spectrum of the planar waveguide at the wavelength of 633 nm was measured by prism coupling equipment with He-Ne laser at Shandong University. The prism coupler used in this paper is Model 2010 produced by Metricon Company in the United States. The end-face coupling technology is an intuitive and effective method for optical waveguides to study guiding properties and propagation losses. To better compare the optical properties of the channel and ridge waveguides, their propagation losses were measured by the end-face coupling method.

3. Results and discussion

The dark-mode spectrum of extraordinary refractive index (n_e) direction for the planar waveguide was measured by prism coupling method after annealing at 260°C for 30 min with a wavelength of 633 nm. A sharp and deep dip is observed in annealed LN planar waveguide, which corresponds to the true propagation mode (TM_0 mode). The effective refractive index (n_{eff} = 2.2124) of TM_0 mode is larger than n_e of the substrate (n_{sub} = 2.2028), which indicates an enhanced index well-formed in the near-surface region for planar waveguide. There were some similar research results on ion-implanted LN waveguide, for example, the n_{eff} values of TM_0 mode were 2.2109 (3 MeV O ion, 1.5×10^{15} ions/cm^2) [23] and 2.2154 (400 keV He ion, 3×10^{16} ions/cm^2) [20]. The differences between the above refractive indices and n_{sub} are within the range of 0.0132, which is the maximum n_e increment at 633 nm supposed in Ref. [25].

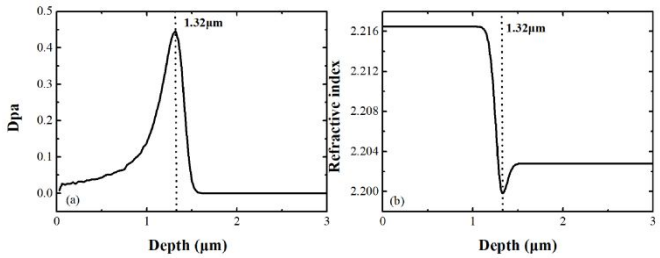

Fig. 2. (a) The dpa profile of 500 keV He ions with the fluence of 1.5 x 10^{16} ions/cm^2 implanted into LN crystal by SRIM 2013; (b) the reconstructed refractive index profile of the LN waveguide after annealing 260°C for 30 min at 633 nm.

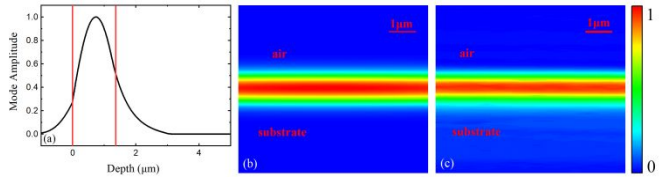

Fig. 3. (a) The profile of TM_0 guided mode simulated by BPM (1D); (b) the modal intensity profile of TM_0 mode computed by the BPM (2D); (c) near-field image of TM_0 mode by use of end-face coupling method.

For integrated optical devices, the refraction index is one of the decisive factors in how propagating light is distributed in the waveguide structure. Given that this is a very critical parameter, we reconstructed the RIP based on dpa profile and the prism coupling measurement results by adjusting the width of two half Gaussians[26]. Fig. 2(a) shows the dpa profile simulated by SRIM 2013. The RIP for n_e direction of the LN waveguide after annealing is shown in Fig. 2(b). The refractive index barrier in Fig. 2(b) is located at 1.32 μm and it is consistent with the damage peak. It indicates that we have fabricated a "well" +

"barrier" type optical waveguide after our He ions implantation process. Based on the RIP in Fig. 2(b), the beam propagation method (BPM) was used to simulate the mode field distribution of planar waveguide after annealing, and the n_{eff} of guide mode was calculated. The region between the two solid red lines is the waveguide region, which is depicted in Fig. 3(a). It can be seen that transverse magnetic (TM) mode can well limit the propagation of light. The calculated n_{eff} for TM_0 mode agrees well with the experimental result, proving that the simulation of the RIP is reasonable. Fig. 3(b) shows the modal intensity profile calculated by the BPM, and we have measured the intensity distribution in the near-field of the planar waveguide under the TM polarization condition after annealing at 260°C in the air for 30 minutes by using the end-face coupling method, as indicated in Fig. 3(c). The measured wavelength is 633 nm. The near field intensity profile under the TE polarization condition was measured also. However, it is too weak to detect. In view of the requirement of propagation loss in practical application, it can be said that the LN planar waveguide prepared in this work can only carry TM_0 mode. As presented in Fig. 3(c), the near-field light intensity distribution presents that most of the light wave energy is limited in the waveguide region. It can be observed that there is a good agreement between Figs. 3(b) and 3(c).

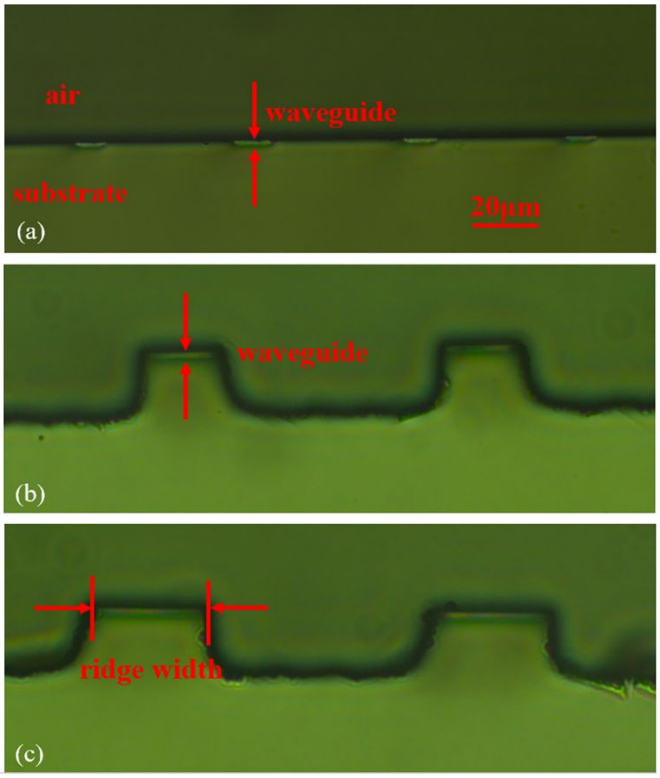

Fig. 4. Optical microscope image (×500) of the end face of waveguides after polishing (a) WG10; (b)WG15; (c) WG25.

The metallographic microscope can be used to measure small changes in the refractive index. We observed the end faces of the WG10, WG15, and WG25 with the Olympus BX51M microscope made in Japan, and all are shown in Figs. 4(a)~4(c), respectively. The bright areas have already been labeled to represent the guidance zones clearly. For WG10, the channel width is ~10 μm and the channel interval is ~40 μm, whereas the ridge widths of the ridge waveguides are respectively available in two sizes, WG15 and WG25, and the ridge depth is ~14 μm, which is much larger than the waveguide layer. As can be seen from Figs. 4(b) and 4(c), it is inevitable to produce edge chipping during the precise diamond dicing process. The existence of the chipping has a certain influence on the quality of the ridge waveguides and the influence decreases with the increase of ridge width.

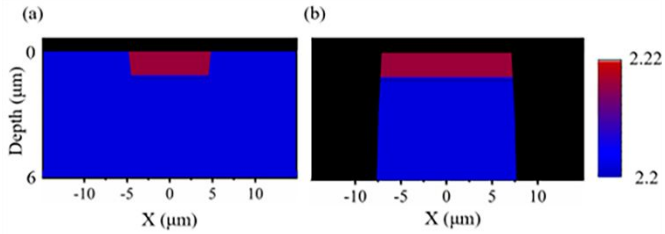

Fig. 5. The reconstructed refractive index profile of the waveguide: (a) WG10; (b) WG15.

For investigating the optical properties of the 2D waveguides prepared, we used different measurement and simulation methods to obtain the refractive index profiles, near-field profiles, and propagation losses. According to the size of the waveguide region obtained under the metallographic microscope in Fig. 4(a), a trapezoidal cross-section of 9 μm for the upper base and 10 μm for the lower base was selected. Considering the trapezoidal cross-section and the planar waveguide RIP shown in Fig. 2(b), the reconstructed RIP of the WG10 is shown in Fig. 5(a). Using the same method, taking the RIP in Fig. 2(b) and the trapezoidal cross-section in Fig. 4(b) into consideration, we calculated the RIP of WG15, and the result is displayed in Fig. 5(b). We only show the reconstructed RIP of WG15 here since the RIP of the ridge shapes of different widths is consistent in the vertical direction.

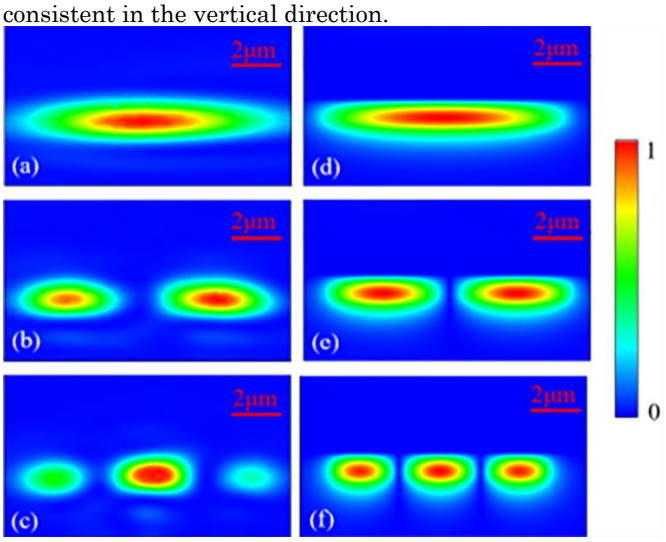

Fig. 6. (a), (b), (c) Near-field image of WG10 quasi-TM modes from the end face of the sample captured by a CCD camera; (d), (e), (f) modal intensity profile computed by FD-BPM is as follows: quasi -- TM_{00}, TM_{10}, TM_{20} modes. The color scale, which represents the relative light intensity is shown also.

The near-field intensity profiles of WG10 and WG15 were measured by the end-face coupling method. During the measurement, one microscope objective (×40) focuses a beam with the wavelength of 633 nm into the waveguide to excite the guided mode, while the other microscope objective (× 40) collects light from the output end face of

the sample, which is imaged onto the CCD camera. It can be seen from Figs. 6 and 7 that the optical waveguides can limit the light in both horizontal and vertical directions, indicating that we have successfully prepared 2D waveguides. The quasi-TM excitation modes (quasi-TM_{00}, quasi-TM_{10}, quasi-TM_{20}) of WG10 and WG15 obtained by the end-face coupling method are shown in Figs. 6(a)~6(c) and Figs. 7(a)~7(c), while the simulation results computed by the BPM are shown in Figs. 6(d)~6(f) and Figs. 7(d)~7(f). The calculation results of WG10 and WG15 are in good agreement with the experimental results, indicating that the waveguides with single mode in the Z direction and multi-mode in the X direction were formed This also proves that the reconstructed RIPs can be consistent with the experiment results.

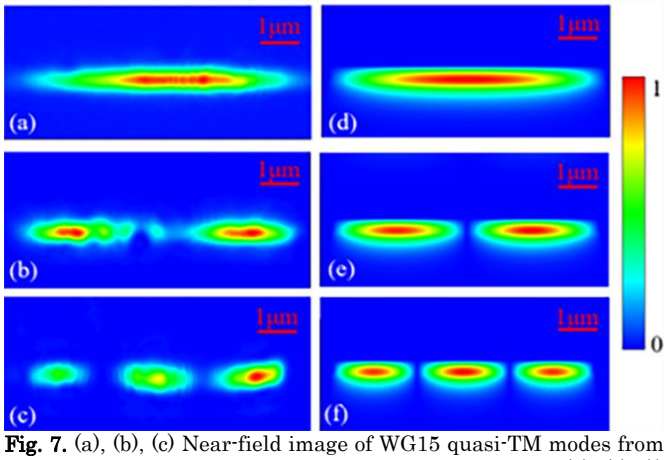

Fig. 7. (a), (b), (c) Near-field image of WG15 quasi-TM modes from the end face of the sample captured by a CCD camera; (d), (e), (f) modal intensity profile computed by FD-BPM. The color scale, which represents the relative light intensity is shown also.

The propagation loss is one of the vital parameters to evaluate the performance of the waveguide. We have used the experimental method to measure the propagation losses of WG10, WG15, and WG25, respectively [27]. Fig. 8 is a scheme of the measurement of the sample propagation loss by the end-face coupling method. The polarization direction of the injected light is controlled by the polarizing film to achieve the desired TM polarization direction. The PM400 Optical Power Meter was employed to measure the power from the input and output end-faces. And BPM was used to estimate the coupling efficiencies of the measured samples. As shown in Table 1, the coupling efficiencies of WG15 and WG25 have a tiny difference due to the difference in waveguide sizes.

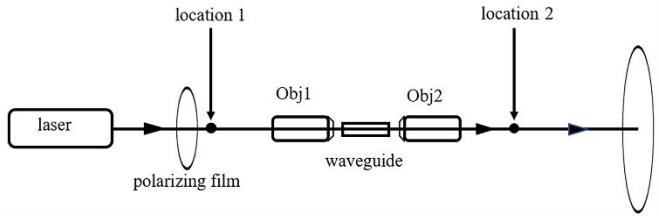

Figure 8. Experimental setup used with the end-fire coupling method. Obj: microscope objective lens; location 1: the position where the light power was first measured; location 1: the position where the light power was second measured.

The propagation losses of the samples are shown in table 1. As one can see, the propagation loss of WG10 is larger than WG25, and the difference in coupling efficiency may be one of the reasons for this result. However, the propagation loss of WG15 is greatly increased compared with that of other waveguides. The roughness of the sidewall that has a greater effect on WG15 may be the reason for this phenomenon. Next, we will further study the propagation losses of ridge waveguides with different widths and explore the factors that affect the propagation losses of ridged waveguides. Lithography and precise diamond dicing technique have their advantages and disadvantages in preparing 2D waveguides. In general, the precise diamond dicing technique is simpler and more environmentally friendly than lithography for 2D waveguides. However, the application scope of precise diamond dicing technology is narrower, which is applied in ridge waveguides most of the time. Lithography can produce a wide variety of 2D waveguides, such as channel waveguides, curved waveguides, branching waveguides, and ridge waveguides. And, through the study of this work, aiming at reducing propagation loss, the lithography is more suitable for 2D waveguides with smaller widths (≤15μm), whereas precise diamond dicing is a better choice to fabricate 2D waveguides with a larger width.

Table 1 The coupling efficiencies and propagation losses of the 2D waveguides at 633 nm for TM polarization.

Waveguide	Coupling efficiency	Propagation loss(dB/cm)
WG10	50.16%	3.42
WG25	46.55%	1.97
WG15	46.72%	12.4

4. Conclusions

In conclusion, the channel waveguide was fabricated by He ion implantation in LN using a slotted photoresist mask to selectively implant the ions in certain areas of the substrate, and the ridge waveguides were prepared by He ion implantation combined with precision diamond dicing. The RIP simulated indicates that we have formed a "well" + "barrier" type optical waveguide. The channel waveguide and ridge waveguides were compared in terms of RIP, light intensity distribution, and propagation loss. For the wavelength of 633 nm, the propagation losses of WG10, WG25, and WG15 are 3.42 dB/cm, 1.97 dB/cm, and 12.4 dB/cm, respectively. As far as we know, the chipping created during the precision diamond dicing process is a factor that affect the propagation loss for ridge waveguides. From our work, we can conclude that the lithography is more suitable with smaller widths (≤15μm) whereas precise diamond dicing is a better choice with a larger width in the preparation of 2D optical waveguides combined with ion implantation technology. This work has a reference value for the application of LN waveguides in integrated photonic devices.

Acknowledgment

This work was supported by the National Science Foundation of China (Grant No. 11805142, 11205096, and 11874243), and the Natural Science Foundation of Shandong Province (Grant No. ZR2020QF086).

References

1. R. Wolf, I. Breunig, H. Zappe, and K. Buse, "Scattering-loss reduction of ridge waveguides by sidewall polishing," Opt. Express **26**, (19815) 2018.

2. Y. Kong, F. Bo, W. Wang, D. Zheng, H. Liu, G. Zhang, R. Rupp, and J. Xu, "Recent Progress in Lithium Niobate: Optical Damage, Defect Simulation, and On-Chip Devices," Adv. Mater. **32**, (e1806452) 2020.
3. S. Y. Siew, E. J. H. Cheung, H. Liang, A. Bettiol, N. Toyoda, B. Alshehri, E. Dogheche, and A. J. Danner, "Ultra-low loss ridge waveguides on lithium niobate via argon ion milling and gas clustered ion beam smoothening," Opt. Express **26**, (4421-4430) 2018.
4. P. R. Sharapova, K. H. Luo, H. Herrmann, M. Reichelt, T. Meier, and C. Silberhorn, "Toolbox for the design of $LiNbO_3$-based passive and active integrated quantum circuits," New J. Phys. **19**, (123009) 2017.
5. I. Krasnokutska, J. J. Tambasco, X. Li, and A. Peruzzo, "Ultra-low loss photonic circuits in lithium niobate on insulator," Opt. Express **26**, (897) 2018.
6. Z. H. Chen, Y. W. Wang, H. H. Zhang, and H. Hu, "Silicon grating coupler on a lithium niobate thin film waveguide," Opt. Mater. Express **8**, (1253) 2018.
7. J. M. Lv, Y. Z. Cheng, J. R. V. de Aldana, X. T. Hao, and F. Chen, "Femtosecond Laser Writing of Optical-Lattice-Like Cladding Structures for Three-Dimensional Waveguide Beam Splitters in $LiNbO_3$ Crystal," J. Lightwave Technol. **34**, (3587) 2016.
8. R. Schiek, A. S. Solntsev, and D. N. Neshev, "Temporal dynamics of all-optical switching in quadratic nonlinear directional couplers," Appl. Phys. Lett. **100**, (111117) 2012.
9. M. R. Zhang, W. Ai, K. X. Chen, W. Jin, and K. S. Chiang, "A Lithium-Niobate Waveguide Directional Coupler for Switchable Mode Multiplexing," IEEE Photon. Technol. Lett. **30**,(1764) 2018.
10. Y. Yao, W. Wang, and B. Zhang, "Designing MMI structured beam-splitter in $LiNbO_3$ crystal based on a combination of ion implantation and femtosecond laser ablation," Opt. Express **26**,(19648) 2018.
11. J. Lv, Y. Cheng, J. R. Vazquez de Aldana, X. Hao, and F. Chen, "Femtosecond Laser Writing of Optical-Lattice-Like Cladding Structures for Three-Dimensional Waveguide Beam Splitters in $LiNbO_3$ Crystal," J. Lightwave. Technol. **34**,(3587-3591) 2016.
12. Q. Zhang, M. Li, J. Xu, Z. Lin, H. Yu, M. Wang, Z. Fang, Y. Cheng, Q. Gong, and Y. Li, "Reconfigurable directional coupler in lithium niobate crystal fabricated by three-dimensional femtosecond laser focal field engineering," Photonics Res. **7**,(503) 2019.
13. P. Aashna, and K. Thyagarajan, "Polarization splitter based on a three waveguide directional coupler using quantum mechanical analogies," J.Opt. **19**,(065805) 2017.
14. F. Chen, and J. R. V. de Aldana, "Optical waveguides in crystalline dielectric materials produced by femtosecond- laser micromachining," Laser Photon Rev. **8**, (251) 2014.
15. C. X. Liu, J. L. You, S. Q. Lin, J. Y. Chen, M. Tang, S. B. Lin, R. L. Zheng, L. L. Fu, and L. L. Zhang, "A ridge waveguide constructed by H^+ implantation and precise diamond blade dicing in high-gain Nd^{3+}-doped laser glass," Optik **225**, (1) 2021.
16. A. Panepinto, D. Cossement, and R. Snyders, "Experimental and theoretical study of the synthesis of N-doped TiO_2 by N ion implantation of TiO_2 thin films," Appl. Surf. Sci. **541**, (148493) 2021.
17. J. Rams, J. Olivares, P. J. Chandler, and P. D. Townsend"Mode gaps in the refractive index properties of low-dose ion-implanted LiNbO3 waveguides," J. Appl. Phys. **87**, (3199) 2000.
18. L. Wan, W. Luo, Y. Yuan, K. Zhang, S. Huang, S. Qiao, X. Pan, and W. Chuangui, "Effects of helium implantation fluence on the crystal-ion-slicing fabrication of Y-cut lithium niobate film," Mater. Express **11**, (717) 2021.
19. N. Cherkashin, N. Daghbouj, G. Seine, and A. Claverie, "Impact of He and H relative depth distributions on the result of sequential He^+ and H^+ ion implantation and annealing in silicon," J. Appl. Phys. **123**, (1) 2018.
20. S. M. Zhang, X. H. Liu, X. F. Qin, K. M. Wang, and X. Liu, "Damage, refractive index and near-field intensity profiles in a single-mode waveguide of $LiNbO_3$ by 400 keV He ion implantation," J. Phys. D: Appl. Phys. **43**, (1) 2010.
21. J. Lin, F. Bo, Y. Cheng, and J. Xu, "Advances in on-chip photonic devices based on lithium niobate on insulator," Photonics Res. **8,** (1910)2020.
22. M. F. Volk, S. Suntsov, C. E. Ruter, and D. Kip, "Low loss ridge waveguides in lithium niobate thin films by optical grade diamond blade dicing," Opt. Express **24**, (1386) 2016.
23. J. H. Zhao, X. S. Jiao, Y. Y. Ren, J. J. Gu, S. M. Wang, M. Y. Bu, and L. Wang, "Lithium niobate planar and ridge waveguides fabricated by 3 MeV oxygen ion implantation and precise diamond dicing," Chin. Opt. Let. **19**, (1) 2021.
24. Y. Cheng, J. Lv, S. Akhmadaliev, S. Zhou, Y. Kong, and F. Chen, "Mid-infrared ridge waveguide in MgO: $LiNbO_3$ crystal produced by combination of swift O^{5+} ion irradiation and precise diamond blade dicing," Opt. Mater. **48**, (209) 2015.
25. H. Hu, F. Lu, F. Chen, B. R. Shi, K. M. Wang, and D. Y. Shen, "Extraordinary refractive-index increase in lithium niobate caused by low-dose ion implantation," Appl. Opt. **40**, (3759) 2001.
26. L. Wang, F. Chen, X.L. Wang, L.L. Wang, K.-M. Wang, L. Gao, H.-J. Ma, and R. Nie, "Si^{2+} ion implanted into stoichiometric lithium niobate crystals: Waveguide characterization and lattice disorder analysis," Nucl. Instrum. Meth. B **251**, (104) 2006.
27. L. Wang, F. Chen, X.-L. Wang, K.-M. Wang, Y. Jiao, L.-L. Wang, X.-S. Li, Q.-M. Lu, H.-J. Ma, and R. Nie, "Low-loss planar and stripe waveguides in Nd^{3+}-doped silicate glass produced by oxygen-ion implantation," J. Appl. Phys. **101** (053112) 2007.